

## Article

# The Effect of Bottom Ash Ball-Milling Time on Properties of Controlled Low-Strength Material Using Multi-Component Coal-Based Solid Wastes

Tianxiang Chen <sup>1</sup>, Ning Yuan <sup>1,\*</sup> , Shanhu Wang <sup>1</sup>, Xinfei Hao <sup>2</sup>, Xinling Zhang <sup>1</sup>, Dongmin Wang <sup>1</sup> and Xuan Yang <sup>1</sup>

<sup>1</sup> School of Chemical and Environmental Engineering, China University of Mining and Technology, Beijing 100083, China

<sup>2</sup> Huayang New Material Technology Group Co., Ltd., Yangquan 045000, China

\* Correspondence: ning.yuan@cumtb.edu.cn

**Abstract:** As the conventional disposal method for industrial by-products and wastes, landfills can cause environmental pollution and huge economic costs. However, some secondary materials can be effectively used to develop novel underground filling materials. Controlled low-strength material (CLSM) is a highly flowable, controllable, and low-strength filling material. The rational use of coal industry by-products to prepare CLSM is significant in reducing environmental pollution and value-added disposal of solid waste. In this work, five different by-products of the coal industry (bottom ash (BA), fly ash, desulfurized gypsum, gasification slag, and coal gangue) and cement were used as mixtures to prepare multi-component coal industry solid waste-based CLSM. The microstructure and phase composition of the obtained samples were analyzed by scanning electron microscopy and X-ray diffraction. In addition, the particle size/fineness of samples was also measured. The changes in fresh and hardened properties of CLSM were studied using BA after ball milling for 20 min (BAI group) and 45 min (BAII group) that replaced fly ash with four mass ratios (10 wt%, 30 wt%, 50 wt%, and 70 wt%). The results showed that the CLSM mixtures satisfied the limits and requirements of the American Concrete Institute Committee 229 for CLSM. Improving the mass ratio of BA to fly ash and the ball-milling time of the BA significantly reduced the flowability and the bleeding of the CLSM; the flowability was still in the high flowability category, the lowest bleeding BAI70 (i.e., the content of BA in the BAI group was 70 wt%) and BAII70 (i.e., the content of BA in the BAII group was 70 wt%) decreased by 48% and 64%, respectively. Furthermore, the 3 d compressive strengths of BAI70 and BAII70 were increased by 48% and 93%, respectively, compared with the group without BA, which was significantly favorable, whereas the 28 d compressive strength did not change significantly. Moreover, the removability modulus of CLSM was calculated, which was greater than 1, indicating that CLSM was suitable for structural backfilling that requires a certain strength. This study provides a basis for the large-scale utilization of coal industry solid waste in the construction industry and underground coal mine filling.

**Keywords:** controlled low-strength material (CLSM); coal industry by-products; bottom ash; bleeding; compressive strength



**Citation:** Chen, T.; Yuan, N.; Wang, S.; Hao, X.; Zhang, X.; Wang, D.; Yang, X. The Effect of Bottom Ash Ball-Milling Time on Properties of Controlled Low-Strength Material Using Multi-Component Coal-Based Solid Wastes. *Sustainability* **2022**, *14*, 9949. <https://doi.org/10.3390/su14169949>

Academic Editor: Dimitrios Komilis

Received: 18 June 2022

Accepted: 9 August 2022

Published: 11 August 2022

**Publisher's Note:** MDPI stays neutral with regard to jurisdictional claims in published maps and institutional affiliations.



**Copyright:** © 2022 by the authors. Licensee MDPI, Basel, Switzerland. This article is an open access article distributed under the terms and conditions of the Creative Commons Attribution (CC BY) license (<https://creativecommons.org/licenses/by/4.0/>).

## 1. Introduction

According to the American Concrete Institute (ACI) Committee 229, controlled low-strength material (CLSM) is a self-compacting and self-leveling cementitious material [1], usually consisting of water, Portland cement, fly ash, and fine aggregate. CLSM can be used in areas that are difficult to access and do not require compression because of its high flowability. The compressive strength of CLSM is designable and determined by whether or not excavation is required in the future. When manual excavation is required, the recommended compressive strength is less than 0.3 MPa, and when mechanical excavation is

required, the recommended compressive strength is between 0.7 and 1.4 MPa. If excavation is not necessary, the recommended compressive strength is less than 8.3 MPa [2,3]. Due to its low strength requirements, CLSM can be perfectly combined with various wastes and by-products obtained locally, thereby reducing costs and improving filling quality [4]. Therefore, CLSM is widely used in geotechnical engineering, such as coal mine fills, pipeline bedding, void fills, etc. Over the years, CLSM has been tested with numerous solid wastes to replace fine aggregates. These include quarry waste [5], treated oil sands waste [6], coal-fired products [7], desulfurization slag [8], etc. To further reduce material costs, some scholars have considered using ground granulated blast-furnace slag [9], dust from asphalt plants [10], waste glass powder [11], calcium carbide slag [12], wastewater sludge [13], etc. to substitute for cement as cementitious materials when producing CLSM. In addition, additives such as foam particles, air-entraining agents, and water-reducing agents can be added to obtain freshly mixed CLSM with high workability.

With the exploitation, processing, and utilization of coal, China produces a great deal of coal-based wastes, such as bottom ash (BA), coal gangue, gasification slag, fly ash, and desulfurized gypsum [14,15]. However, these coal-based solid wastes are generated, stockpiled, and not effectively utilized, which causes serious ecological damage and environmental pollution [16,17]. In order to address this problem, some researchers have developed a series of coal-based solid wastes resource utilization approaches [18–20], including the preparation of functional materials from wastes, coal gangue power generation, agricultural application, valuable element recovery, and so forth. However, as China's economic development gradually enters the new normal, the demand for traditional building materials such as cement and concrete has decreased in the building materials industry [21]. This makes the comprehensive utilization of coal-based solid waste face severe challenges. If CLSM prepared from multi-component coal-based solid wastes can be applied to underground filling on a large scale, it can not only reduce the threat to the environment but also make reasonable use of solid wastes, resulting in huge economic benefits.

Using solid wastes and improving their comprehensive utilization rate is important in China's current ecological and environmental protection work. BA is the solid waste discharged from the bottom of a boiler after coal combustion in a power plant. The BA is mainly irregular with smooth edges and corners, mainly composed of  $\text{SiO}_2$ ,  $\text{Al}_2\text{O}_3$ ,  $\text{CaO}$ , and  $\text{Fe}_2\text{O}_3$ , accounting for about 90%, and belongs to silicon-alumina materials [22]. BA has good pozzolanic activity and can be used as a concrete admixture after being optimized by fine grinding or chemical modification [23,24]. For example, Pakawat et al. studied the variation of notch size particles on BA pozzolanic activity, and the results showed that the compressive strength values of mortar prepared with BA were 5% and 14% higher than that of mortar using 100% Portland cement at 28 d and 60 d of curing ages, respectively. The high pozzolanic activity of BA exhibited great potential as a cement substitute [25]. Additionally, Belén et al. used ground ash as a cement additive and compared its performance with that of limestone as an additive. The results showed that the compressive strength of cement with 40 wt% BA was higher than that of standard cement and limestone as additives. Furthermore, cement with 20 wt% BA can save 9% clinker against commercial cement (CEM II/AL 42.5 R), and cement with 40 wt% BA can save 14% clinker against commercial cement (CEM II/BL 32.5 N) [26]. Although BA has been utilized in cement and concrete, the utilization rate of BA and other wastes is not enough in general and needs to be improved.

In addition, researchers also selected other coal-based solid wastes for utilization [27]. Kaliyavaradhan et al. reviewed the effects of solid wastes such as circulating fluidized bed combustion ash, ponded ash, slag, and BA on the strength of CLSM and suggested the mixing ratio of the mixed waste in CLSM [28]. Ling et al. outlined the research development and practical application of CLSM in trench backfilling and found through 115 pieces of literature from various countries around the world that the materials used to produce CLSM vary from country to country. This will affect the nature of CLSM production and have significant implications for practical applications in the field [29]. Specifically, Zhang et al. used fly ash and coal gangue as raw materials to study the feasibility of

filling. When the mass ratio of coal gangue:fly ash:cement was 14:5:1, the filling body not only had good fluidity but also could meet the requirements of compressive strength and dehydration [30]. With the development of CLSM, more kinds of solid waste are required to be added to the preparation of CLSM. For example, Yang et al. prepared composites using desulfurized gypsum, low-calcium fly ash, slag, and cement as cementitious materials and total tailings as aggregates and conducted a filling test. It is noted that when the fly ash content is high, the prepared composite materials can meet the strength requirements of mine filling [31]. The use of a wider variety of solid wastes is an effective solution to minimize the environmental problems associated with the disposal of these wastes.

At present, although CLSM based on the coal industry by-products has been investigated extensively, the research on the preparation of CLSM aiming at fully utilizing the five kinds of coal-based solid wastes remains scarce. In this work, for the first time, we mixed these five coal-based solid wastes with cement for the purpose of underground filling. In addition, in order to further reduce the bleeding of CLSM and improve the early strength of CLSM, the BA was ground. By changing the grinding time of the BA, we studied the effect of different ball-milling of BA on the flowability, bleeding, compressive strength (3 d, 7 d, and 28 d), fresh density, dry density, setting time, porosity, absorption, and microstructure of CLSM in detail. The preparation of this CLSM can not only reduce the environmental protection tax levied by some enterprises for stacking coal-based solid waste and reduce the burden on enterprises but also solve the current ecological and environmental problems caused by the inability to properly handle coal-based solid wastes. Specifically, in the obtained CLSM, BA, desulfurized gypsum, fly ash, and cement were employed as cementitious materials, and coal gangue and gasification slag were utilized as aggregates. BA with ball-milling times of 20 min and 45 min was used to replace fly ash in different mass ratios (i.e., 10 wt%, 30 wt%, 50 wt%, 70 wt%), and the changes in fresh and hardened properties of CLSM were investigated. The crystallinity and composition of the hydration products were characterized by X-ray diffraction (XRD), and the microstructure of CLSM was characterized by scanning electron microscopy (SEM).

## 2. Experimental Programs

### 2.1. Materials

The cement employed in the experiment is the benchmark cement PI 42.5 Portland cement. The chemical compositions of all coal-based solid wastes and cement are shown in Table 1, and their XRD characterizations are provided in Figure 1. The admixture used in the experiment is a powdered polycarboxylate superplasticizer.

**Table 1.** Chemical compositions of coal-based solid wastes and cement (wt%).

| Compound                       | Cement | Bottom Ash | Fly Ash | Desulfurized Gypsum | Gasification Slag | Coal Gangue |
|--------------------------------|--------|------------|---------|---------------------|-------------------|-------------|
| SiO <sub>2</sub>               | 20.72  | 56.37      | 52.95   | 2.62                | 48.07             | 48.46       |
| Al <sub>2</sub> O <sub>3</sub> | 4.62   | 26.71      | 27.55   | 0.58                | 16.37             | 24.13       |
| CaO                            | 62.18  | 3.41       | 4.94    | 28.77               | 8.95              | 0.10        |
| Fe <sub>2</sub> O <sub>3</sub> | 3.26   | 6.62       | 6.31    | 0.43                | 8.84              | 9.44        |
| MgO                            | 3.15   | 1.20       | 1.92    | 2.46                | 1.91              | 0.47        |
| Na <sub>2</sub> O              | 0.52   | 1.08       | 1.52    | 0.25                | 1.77              | 0.25        |
| K <sub>2</sub> O               | 0.34   | 1.58       | 1.85    | 0.12                | 1.48              | 1.99        |
| TiO <sub>2</sub>               | —      | 1.04       | 1.28    | 0.03                | 0.90              | 0.86        |
| SO <sub>3</sub>                | 2.72   | 0.47       | 1.03    | 40.17               | 0.61              | 0.09        |
| f-CaO                          | 0.72   | —          | —       | —                   | —                 | —           |
| Cl <sup>−</sup>                | 0.012  | —          | —       | —                   | —                 | —           |
| Loss                           | 1.84   | 1.09       | 0.19    | 24.50               | 10.30             | 14.03       |

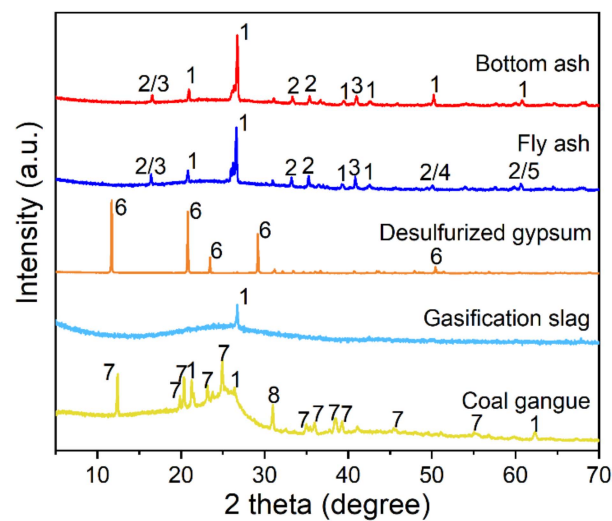


**Figure 1.** XRD patterns of bottom ash, fly ash, desulfurized gypsum, gasification slag, and coal gangue. Components: 1-SiO<sub>2</sub>, 2-3Al<sub>2</sub>O<sub>3</sub>·2SiO<sub>2</sub>, 3-Al<sub>2</sub>[SiO<sub>4</sub>]O, 4-Fe<sub>2</sub>O<sub>3</sub>, 5-CaO, 6-CaSO<sub>4</sub>(H<sub>2</sub>O)<sub>2</sub>, 7-Al<sub>2</sub>Si<sub>2</sub>O<sub>5</sub>(OH)<sub>4</sub>, 8-FeS<sub>2</sub>.

BA used in the experiment is from Yuanyang Lake Power Plant in Ningxia, China. It can be seen in Figure 2 that the particle size of the BA changes after ball milling. After 20 min of ball milling, the particle size of the BA basically reaches 100 μm or less. When the ball milling time is increased to 45 min, the coarse BA is further crushed and refined, and the *d*<sub>50</sub> decreases from 26.3 μm to 13.2 μm. It is close to fly ash particle size, but it is still larger than the latter. Further increasing the ball milling time, the proportion of fine particles will continue to increase. However, at the same time, the cost of the ball-milling process will increase exponentially. After comprehensive consideration, the ball-milling times of 20 min and 45 min are used for the pretreatment of BA in the experiment. Figure 3a presents the microstructure and morphology of the BA, which is mainly composed of irregular block particles with large differences in particle size, and the block particles display a porous surface.

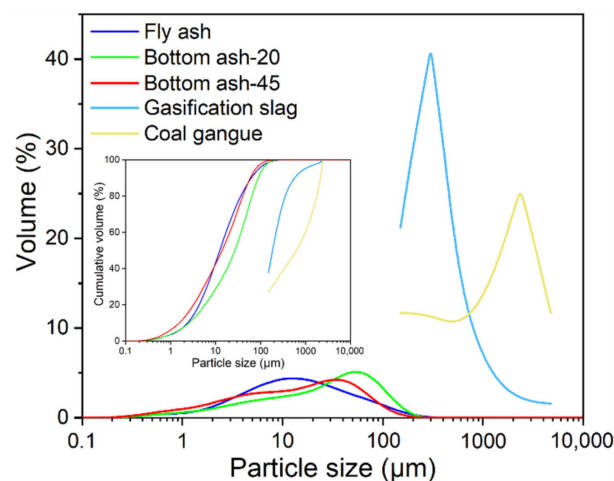


**Figure 2.** Particle size distributions of bottom ash at different ball-milling times (20 min, 45 min), fly ash, gasification slag, and coal gangue.

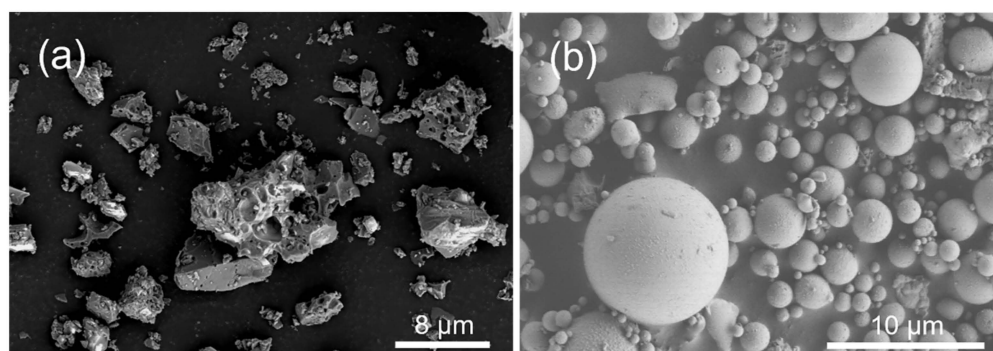


**Figure 3.** SEM analysis of (a) bottom ash and (b) fly ash.

Fly ash is the fine ash collected during the purification of flue gas in the second phase at the Yuanyang Lake Power Plant in Ningxia, China. According to Figure 2, the characteristic parameter of fly ash particle size  $d_{10}$ ,  $d_{50}$ , and  $d_{90}$  are 2.51  $\mu\text{m}$ , 13.18  $\mu\text{m}$ , and 69.18  $\mu\text{m}$ , respectively. Figure 3b presents the microstructure and morphology of fly ash, indicative of spherical particles.

The desulfurization gypsum is from the Yuanyang Lake Power Plant in Ningxia, China. It can be seen in Figure 1 that there is no other mineral phase except dihydrate gypsum, and the phase composition is almost single. The gasification slag used in the experiment is the coarse gasification slag from the Ningxia Coal Mine. The sieving results of the gasification slag are shown in Figure 2. The fineness module of the gasification slag is 1.73, and the particles between 0.15–0.6 mm account for 75%, which can be classified as fine sand. The coal gangue used in the experiment is the original gangue from the Renjiazhuang Coal Mine in Ningxia. It is crushed into gangue particles with a maximum particle size of less than 4.75 mm by the secondary jaw crusher. The crushed coal gangue is screened and analyzed, as shown in Figure 2, and it is found that the content of particles larger than 4.75 mm in the crushed coal gangue is only 11.7%. After further sieving analysis of particles smaller than 4.75 mm, it is found that in the crushed coal gangue smaller than 4.75 mm and the content of particles smaller than 0.15 mm reaches 15.3%. The fineness module of coal gangue is 2.83, which can be recognized as medium sand.

## 2.2. Mixture Proportions

The CLSM mixture proportions are shown in Table 2. Fly ash and two types of BA are used as the main cementitious materials to prepare CLSM mixtures, and the CLSM mixtures are divided into two groups: BAI group (BA with ball milling time of 20 min) and BAII group (BA with ball milling time of 45 min), to investigate the effect of the two types of BA on the CLSM mixture's performance. According to the recommendation of ACI Committee 229 [1], binder–aggregate ratios are lightly adjusted. The proportion of each aggregate and each cementitious material is determined according to previous research in our laboratory. Firstly, 60 wt% coal gangue (total solid mass of mixture) and 15 wt% gasification slag (total solid mass of mixture) are determined as fine aggregates, the ratio of aggregate to cementitious material is kept at 3:1, and the amounts of cement and desulfurized gypsum are 5 wt% and 1 wt%, respectively. Afterward, 10 wt%, 30 wt%, 50 wt%, and 70 wt% of the fly ash are replaced with BA according to the mass of the fly ash. The mixtures are named Blank, BAI10, BAI30, BAI50, BAI70, BAII10, BAII30, BAII50, and BAII70 according to the type and weight of the added BA, as shown in Table 2.

## 2.3. CLSM Preparation and Testing Procedure

All materials used in the experiments were naturally dried before use. Next, CLSM is prepared according to the mixture proportions (Table 2) and the mixing program. The ingredients were mixed for 1 min without adding water in a cement mortar mixer (Shanghai INESA Scientific Instrument, JJ-15 type) to ensure uniform distribution. Thereafter, the mixed water was divided in half. The first half of the mixed water and the polycarboxylate

water-reducing agent were gradually added to the mixture while continuing to mix and stir for 1 min. Then, the second half of the mixed water was added, mixed, and stirred for 1 min. After all the mixed water was added, the mixture was allowed to stand for 1 min and then mixed for 2 min. The fresh mortar specimen was introduced into a mold of 70.7 mm × 70.7 mm × 70.7 mm. The mold was removed after 36 h, and the mortar specimen was cured in a standard curing room (SHBY-40B type, Cangzhou Huaxi, temperature 20 ± 1 °C, humidity above 95%) for 3 d, 7 d, and 28 d. All performance test standards are shown in Table 3.

**Table 2.** Experimental scheme of CLSM.

| Mixture | Aggregate (kg m <sup>-3</sup> ) |                   | Cementitious Materials (kg m <sup>-3</sup> ) |         |            |                     | Water (kg m <sup>-3</sup> ) | Water-Reducing Agent (kg m <sup>-3</sup> ) |
|---------|---------------------------------|-------------------|--|---------|------------|---------------------|-----------------------------|--|
|         | Coal Gangue                     | Gasification Slag | Cement                                       | Fly Ash | Bottom Ash | Desulfurized Gypsum |                             |  |
| Blank   | 960                             | 240               | 80   | 304     | 0          | 16                  | 280                         | 0.8  |
| BAI10   | 960                             | 240               | 80   | 273.6   | 30.4       | 16                  | 280                         | 0.8  |
| BAI30   | 960                             | 240               | 80   | 212.8   | 91.2       | 16                  | 280                         | 0.8  |
| BAI50   | 960                             | 240               | 80   | 152     | 152        | 16                  | 280                         | 0.8  |
| BAI70   | 960                             | 240               | 80   | 91.2    | 212.8      | 16                  | 280                         | 0.8  |
| BAII10  | 960                             | 240               | 80   | 273.6   | 30.4       | 16                  | 280                         | 0.8  |
| BAII30  | 960                             | 240               | 80   | 212.8   | 91.2       | 16                  | 280                         | 0.8  |
| BAII50  | 960                             | 240               | 80   | 152     | 152        | 16                  | 280                         | 0.8  |
| BAII70  | 960                             | 240               | 80   | 91.2    | 212.8      | 16                  | 280                         | 0.8  |

**Table 3.** Standards for the testing methods.

| Test Procedure                        | Standard        | References |
|---------------------------------------|-----------------|------------|
| Flowability                           | ASTM D6103-17   | [32]       |
| Bleeding and fresh density            | GB/T 50080-2016 | [33]       |
| Compressive strength                  | GB/T 50081-2019 | [34]       |
| Setting time                          | GB/T 1346-2011  | [35]       |
| Absorption, porosity, and dry density | ASTM D6023-16   | [36]       |

ASTM-American Society for Testing and Materials; GB-China National Standard.

#### 2.4. Microstructure Testing

X-ray diffraction (XRD) was acquired on a Rigaku Mini Flex 600 powder diffractometer using a Cu-K $\alpha$  target ( $\lambda = 1.5406 \text{ \AA}$ ) with a test voltage of 40 kV and a test current of 15 mA. The obtained diffraction pattern was compared with the standard pattern, and the composition of the sample was determined according to the position of the diffraction peak. The particle size/fineness analysis was performed using a Malvern Mastersizer 2000 laser particle size analyzer. The morphology and hydration products of the solid wastes were scanned using a cold field emission scanning electron microscope (ZEISS Gemini 300) at 25 °C with a cold field emission electron source, accelerating voltage of 0.5–30 kV and accelerating current of 10 mA.

### 3. Results and Discussion

#### 3.1. Flowability

The flowability results for tested CLSM mixtures are shown in Figure 4. The flowability for all mixtures is between 193–280 mm. According to ACI Committee 299 [1], except for BAI70, all CLSM mixtures fall into the high flowability category. Compared with the Blank group, the flowability declines with the rise in both BA contents. This is because the shape of the BA particles is irregular and cannot function as a "ball bearing", which increases the internal friction between the particles [37]. At the same time, the pore volume of BA is larger than that of fly ash, and the rise in BA will cause more water to be absorbed into the inner pores of BA and reduce the flowability [38]. Furthermore, the flowability of the BAI group is slightly lower than that of the BAI group, which is due to the fact that with the

rise in ball milling time, the BA particles become finer, which rises the pore volume and specific surface area, resulting in lower flowability [39,40]. This is also confirmed in the bleeding experiment results.

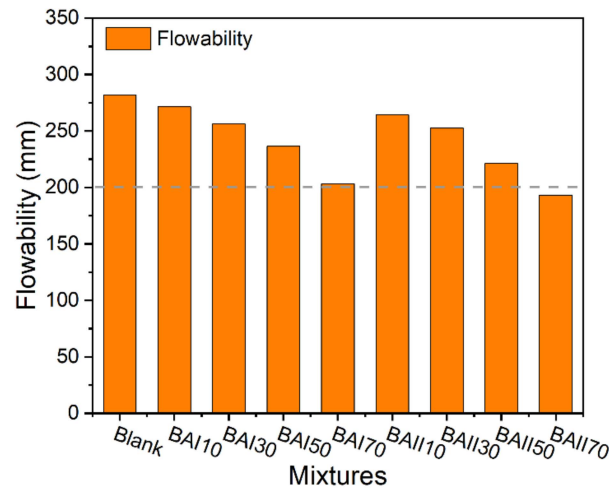


**Figure 4.** Flowability of various CLSM mixtures.

### 3.2. Bleeding

All bleeding results for the tested CLSM mixtures are shown in Figure 5. It can be confirmed that the CLSM does not exceed the 5% requirement recommended by ACI Committee 229 [1]. The bleeding value of the CLSM mixture declines with the rise in BA content. The bleeding values of BAI10, BAI30, BAI50, and BAI70 are 2.70%, 2.15%, 1.99%, and 1.53%, respectively, whereas the bleeding values of CLSM mixtures of BAI110, BAI330, BAI150, and BAI170 are 2.17%, 1.65%, 1.46%, and 1.05%, respectively, which are lower than 2.92% in the Blank mixture. Especially, BAI70 and BAI170 present a significant decrease of 48% and 64% in bleeding, respectively. There are two reasons for the reduction in bleeding. Firstly, the BA has a large particle size and rough and porous surface, which entitles the BA to a higher water-holding capacity [41], and secondly, the addition of BA reduces the morphological effect and micro-aggregate effect of fly ash. Because the shape of fly ash particles is suitable and the surface is smooth and dense, CLSM can obtain good water reduction. Simultaneously, gaps are formed between particles to prevent agglomeration between particles. However, this results in more permeable water from the CLSM, thus higher bleeding [42].

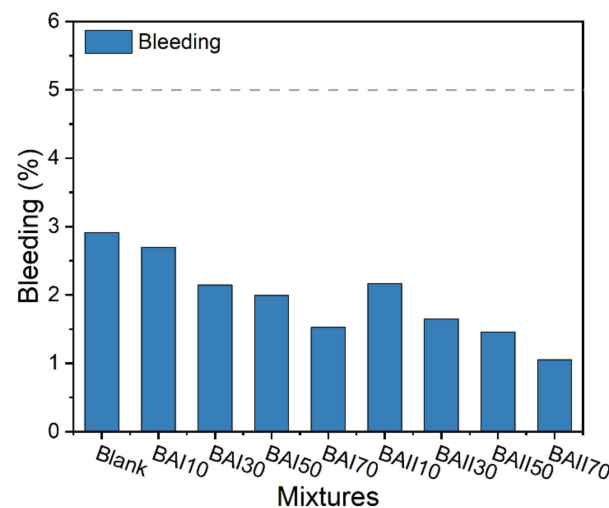


**Figure 5.** Bleeding of various CLSM mixtures.

In addition, when the mass ratio remains unchanged, the bleeding of the mixture of the BAII group is lower than that of the mixture of the BAI group. With the increase in BA ball milling time, finer BA particles result in a larger specific surface area and pore volume, an increase in water holding capacity, and a reduction of water exudation [43]. As a consequence, it can be concluded that the coarse and porous BA can absorb more water during the CLSM mixing process, which will reduce the exudation of water in the CLSM mixture. This phenomenon has also been observed in previous research [7,44,45].

### 3.3. Density

The density of the fresh and hardened CLSM samples at 28 d is determined, as displayed in Figure 6. The fresh density of CLSM ranges from  $1940 \text{ kg m}^{-3}$  to  $2023 \text{ kg m}^{-3}$ . Compared with the blank group, the fresh density of CLSM with BA is increased or decreased but still within the normal CLSM range (i.e.,  $1842 \text{ kg m}^{-3}$ – $2323 \text{ kg m}^{-3}$ ) reported by the ACI Committee 229 [1]. The BA with a long ball-milling time adsorbs more water. Therefore, with the same mass ratio, the fresh density of the BAII group is higher than that of the BAI group. This is also in line with the measurement results of bleeding.

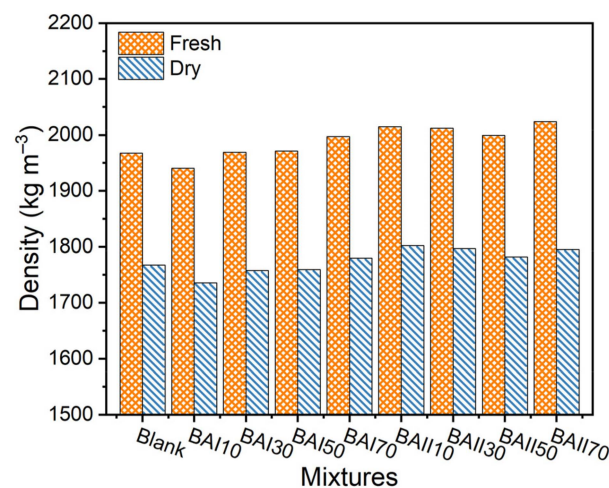


**Figure 6.** Fresh density and dry density test results of CLSM mixtures.

It can be seen that for all tested CLSM mixtures, the dry density is lower than the fresh density due to the loss of water in the CLSM samples [46]. Moreover, the dry density is consistent with the changing trend of the fresh density. The dry density of CLSM is between  $1735 \text{ kg m}^{-3}$  and  $1801 \text{ kg m}^{-3}$ , which is basically in line with CLSM requirements (i.e.,  $1762 \text{ kg m}^{-3}$ – $1890 \text{ kg m}^{-3}$ ) [1].

### 3.4. Compressive Strength

Figure 7 exhibits the compressive strength (3 d, 7 d, and 28 d) and removability modulus (RE) of CLSM. It can be seen that the compressive strength does not exceed the upper limit (8.3 MPa) recommended by the ACI Committee 229. When the amount of BA is the same, the compressive strength (3 d) of the CLSM mixture BAII group is higher than that of the BAI group (Figure 7a). Compared with Blank, as the amount of BA rises, the BAI group increases by 4%, 7%, 16%, and 48%, respectively, and the BAII group increases by 8%, 16%, 60%, and 93%, respectively. This can be explained as follows. The water absorption of BA is higher than that of fly ash, and the BA reduces the free water in the freshly mixed CLSM, which is helpful for the improvement of early strength [47]. Meanwhile, the high content of  $\text{SiO}_2$  in the BA leads to the initial production of many calcium silicate hydrates (C-S-H) [38,48,49], resulting in a high early compressive strength of the CLSM prepared from the BA.

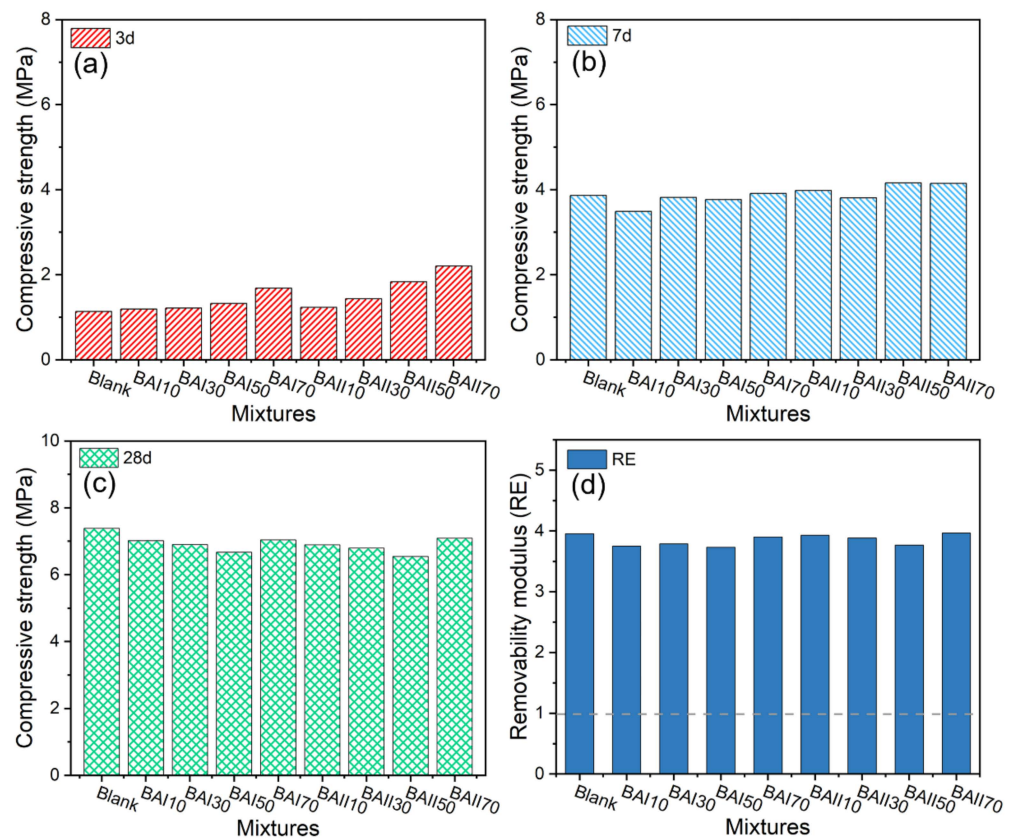


**Figure 7.** Compressive strength of CLSM mixtures at (a) 3 d, (b) 7 d, (c) 28 d, and (d) calculated results of removability modulus (RE).

With the rise in curing time, the development speed of strength (7 d) of CLSM with BA decreases and will tend to be consistent with the Blank group, but the trend of BAI > BAI > Blank can still be observed, as shown in Figure 7b. This is because the hydration reaction continues, the structure of the slurry becomes denser, and the non-homogeneity [7] of the CLSM containing BA begins to manifest, resulting in a decline in the speed of strength development. Compared with the BAI group, the BAI group possesses higher strength at 3 d and 7 d because the BAI group has an enhanced specific surface area and pozzolanic activity [26] after a long time of ball milling, and, thus, the formation of C-S-H gel is promoted. The aforementioned changes in compressive strength are consistent with previous studies [50]. In particular, in contrast to the blank group, the compressive strength of the BAI group exhibits a trend of first decreasing and then increasing, and the same trend can be observed in the BAI group. The lowest point of compressive strength in the BAI group appears when the BA content is 10% (BAI10), whereas the lowest value of compressive strength in the BAI group emerges with a BA content of 30% (BAI30). The occurrence of the lowest point moves backward. This is because the increase in the BA ball milling time (i.e., the decrease in bottom ash particle size) makes the non-homogeneity of CLSM only start to appear obvious after the content of BA is increased.

Finally, as shown in Figure 7c, it is observed that the compressive strength of CLSM at 28 d showed a change of Blank > BAI > BAI, and with the rise in BA, the 28 d compressive strength showed a trend of first declining and then rising. The reason for this change is that the pozzolanic activity of BA is not as high as that of fly ash, which contributes less to the compressive strength of CLSM in the later stage of curing, and the non-homogeneity of CLSM has a negative impact on the compressive strength. Therefore, the compressive strength of CLSM with BA is lower. It is worth noting that the mixtures containing 70 wt% BA have a higher 28 d compressive strength, which may be due to the large rise in BA

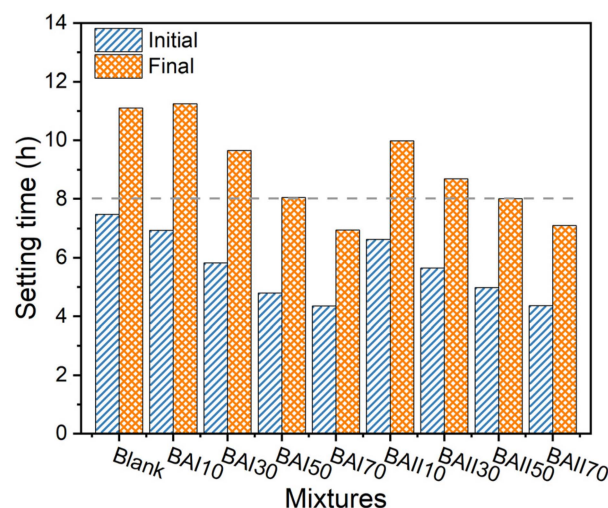
content will lead to the decrease in CLSM non-homogeneity and the increase in CLSM compactness and, thus, the enhancement of compressive strength.

Figure 7d shows the removability modulus (RE) values for all tested CLSM mixtures. RE can be calculated according to Equation (1), based on the 28 d compressive strength ( $C$ ) (kPa) and dry density ( $W$ ) ( $\text{kg m}^{-3}$ ). The RE value is used to evaluate the excavatability of CLSM mixtures. Structural filling applications require the CLSM to have sufficient load-carrying capacity. However, for projects that require later excavation, keeping the low strength is a major goal. Some early acceptable mixtures continue to build in strength over time, making future excavations difficult. BA has little effect on the removability modulus, with RE above 1 for all samples. Therefore, the operation of manually excavating these CLSM mixtures is difficult, and it is suitable for structural fills where certain strength is required [6,51].

$$RE = \frac{0.619 \times W^{1.5} \times C^{0.5}}{10^6} \quad (1)$$

### 3.5. Setting Time

For applications such as backfills, void filling, and structural fills, it is necessary to measure the setting time required by the CLSM to allow people or items to move over the CLSM surface. The maximum acceptable limit for the initial setting time of the CLSM mixture is 36 h. As shown in Figure 8, the initial setting time of our prepared CLSM mixture is between 4.35 and 7.48 h, which are all lower than the general CLSM requirements [52]. It is found that the increase on BA content accelerates the initial setting time of CLSM, which is the same as the results of previous studies [53,54]. The ball-milling time of BA exerts no significant effect on the initial setting time. Furthermore, the final setting time also declines significantly with the rise in BA content. The final setting time of BAI70 and BAI170 is reduced by 37% and 36%, respectively. The main reason for this phenomenon is that aluminum, silicon, and calcium can be leached more easily from BA than from fly ash [55], and C-S-H gel can also be formed more quickly, while the C-S-H gel plays a key role in the solidification behavior of CLSM. Therefore, this may be the reason why the initial and final setting time of CLSM decline with the rise in BA content.



**Figure 8.** Initial and final setting time of prepared CLSM mixtures.

### 3.6. Absorption and Porosity

Absorption and porosity were tested at 28 d, and the data are depicted in Figure 9. The absorptivity of the CLSM mixtures is in the range of 13.5–14.9%, and the porosity is in the range of 11.9–13.0%, both of which increase with the rise in BA content. This is due to the fact that the pozzolanic activity of the BA is less than that of fly ash, resulting in less C-S-H gel produced, which cannot fill the macropores in the CLSM, thus forming an open microstructure [46].

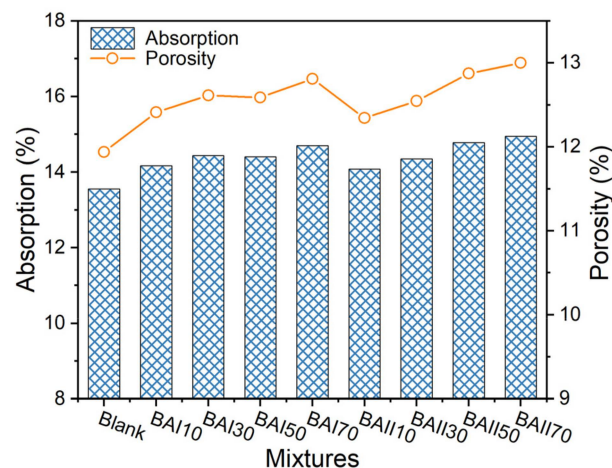


**Figure 9.** Absorption and porosity test results of prepared CLSM mixtures.

### 3.7. Microstructure

Figure 10a–f are the SEM images of CLSM at 28 d, showing the micro-interface properties of Blank, BAI30, BAI70, BAI130, and BAI170. It can be observed that unreacted fly ash microspheres are embedded in the gel phase and aggregates since fly ash particles of different sizes are spherical and easy to identify [46]. The existence of unreacted fly ash particles is caused by the excessive silica content in the system, which is further proved by the XRD results.

The presence of a large number of pores can be observed in Figure 10c–f. On the one hand, this is because the BA is a porous microstructure, which gives rise to high water absorption. The higher initial water content will lead to more voids during the hardening stage. On the other hand, this is due to the fact that the pozzolanic activity of BA is not as good as that of fly ash, and the hydration process produces less C-S-H gel, which cannot fill the macropores in CLSM, and finally forms an open microstructure with high porosity [37]. Compared with BAI70 and BAI170, the structures of BAI30 and BAI130 are slightly denser. This is also consistent with the test results of absorption and porosity.

Figure 11 presents the XRD patterns of the CLSM curing age of 28 d, in which diffraction peaks assigned to quartz, ettringite, C-S-H, and dehydrated gypsum can be observed [45,52]. Weak peaks (i.e., low-intensity peaks) for C-S-H and ettringite can be discovered in all CLSM samples. The hydration reaction produces ettringite and C-S-H, while quartz and gypsum crystals still exist as minerals themselves, presumably from fly ash, BA, and desulfurized gypsum. The incompletely reacted cementitious materials (such as fly ash) can also be found in the test blocks. These findings can also be demonstrated by SEM results. The quartz peak at  $26.6^\circ$  is dominant in the CLSM mixture. The quartz diffraction peaks of BAI170 and BAI70 are significantly stronger than that of Blank, BAI130, and BAI30. This is because the  $\text{SiO}_2$  content in the chemical composition of the BA is higher than that in the fly ash, and the increase in the content of the BA will also lead to a gradual rise in the content of  $\text{SiO}_2$ . The ettringite and C-S-H peak intensities of the CLSM samples with more BA content are lower. This is because the amount of fly ash is negatively correlated with the amount of BA, and the decline in fly ash leads to a decline in the level of hydration reaction that produces C-S-H, resulting in a decrease in the intensity of the C-S-H peak.

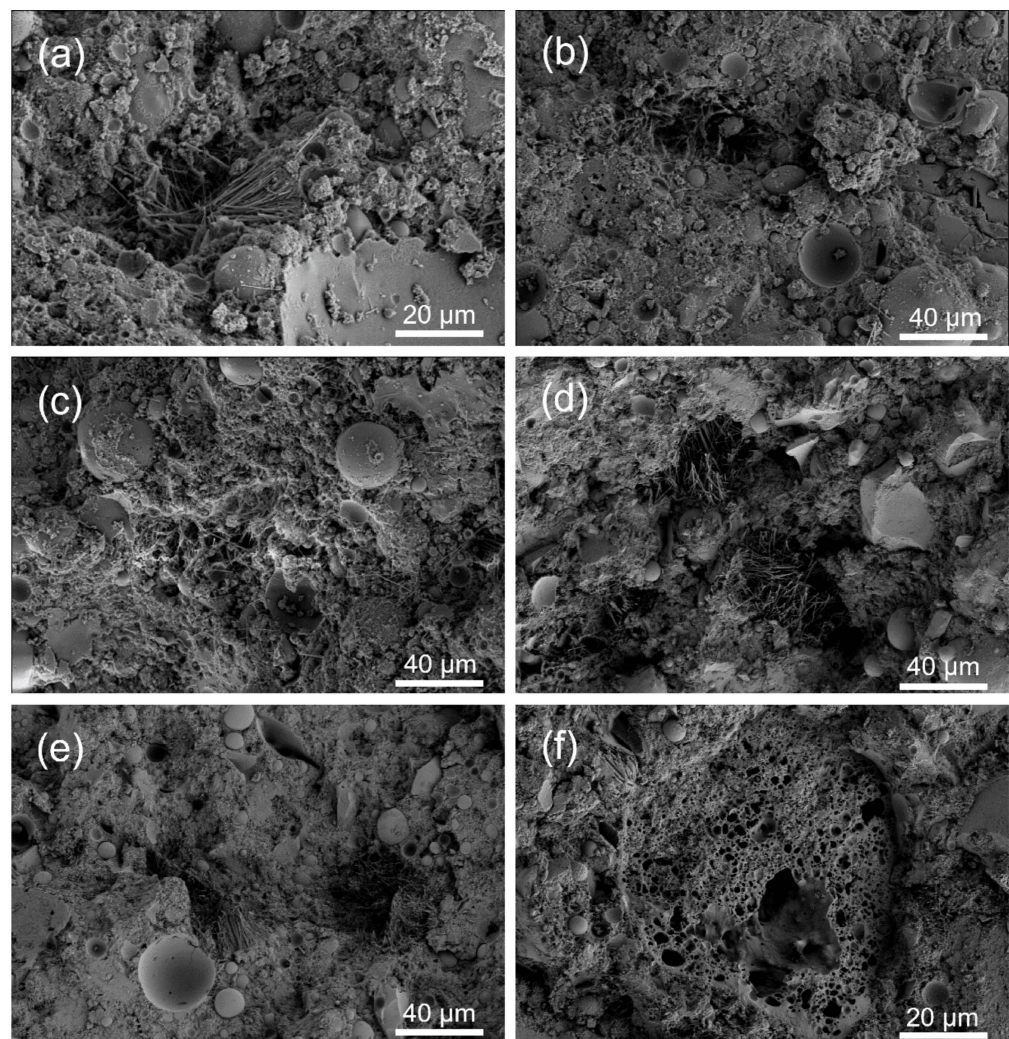


**Figure 10.** SEM images of prepared CLSM mixtures. (a,b) Blank, (c) BAI30, (d) BAI70, (e) BAI30, (f) BAI70.

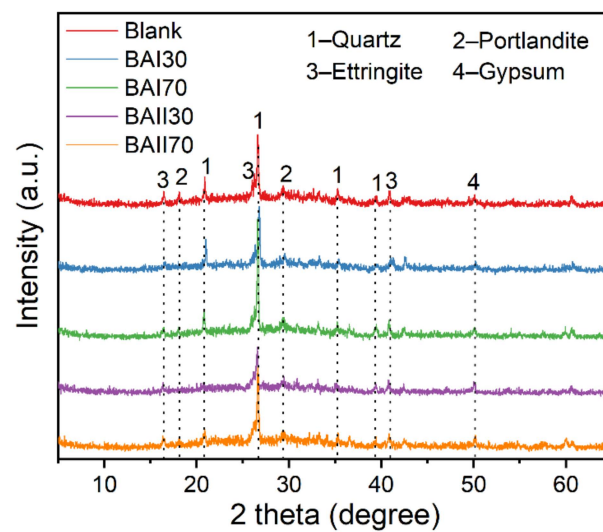


**Figure 11.** XRD patterns of prepared CLSM mixtures at 28 d: Blank, BAI30, BAI70, BAI30, and BAI70.

#### 4. Conclusions

The present work shows that the use of five different by-products and cement to produce CLSM is very feasible. Furthermore, the effects of increasing the amount of BA and increasing the BA ball milling time on the fresh and hardened properties of CLSM are investigated, respectively. The performance of some CLSM was enhanced by increasing BA content and increasing the BA ball milling time. The conclusions of this study can be summarized as follows.

- (1) The flowability, bleeding, compressive strength, setting time, density, porosity, and absorption of CLSM met the specification and requirements of ACI Committee 229. The flowability and bleeding of CLSM decreased with the increase in BA content and ball milling time. However, the flowability was still in the high flowability range, and the reduction in bleeding was favorable. Bleeding was reduced by 48% and 64% for BAI70 and BAI70, respectively. The density, porosity, and absorption of CLSM did not change significantly with the addition of BA and the change in ball-milling time. With the increase in BA content, the initial setting time and final setting time of CLSM declined significantly, and the final setting time of BAI70 and BAI70 decreased by 37% and 36%, respectively.
- (2) The addition of BA and the increase in ball-milling time improved the 3 d strength of CLSM. Compared with Blank, BAI70 and BAI70 increased by 48% and 93%, respectively, which was favorable for structural fills. With the increase in the mass ratio, the 7 d and 28 d strength showed a trend of first declining and then increasing, but the fluctuation was not remarkable. The RE values of all CLSM mixtures were all greater than 1, which is suitable for structural fills that require a higher strength.
- (3) It was observed in the SEM images that the BA-containing CLSM exhibited an open microstructure with high porosity. As revealed by XRD, with the rise in BA content, the quartz peaks of CLSM samples were enhanced, whereas the intensities of ettringite and C-S-H peaks were reduced.
- (4) The production of CLSM with coal-based solid wastes as raw materials is feasible in terms of engineering performance, cost, and environmental impact. In the future, research on cement-free CLSM for total solid wastes should be strengthened to further reduce costs. Additionally, considering the location, utilization rate, and economy of raw materials, the feasibility of large-scale production and application of the CLSM prepared in this work for underground filling should be discussed.

**Author Contributions:** Conceptualization, T.C., N.Y. and S.W.; methodology, N.Y. and S.W.; validation, T.C. and S.W.; formal analysis, T.C., X.Z. and S.W.; investigation, T.C. and S.W.; resources, N.Y., X.H. and D.W.; data curation, T.C., N.Y. and S.W.; writing—original draft preparation, T.C., N.Y. and S.W.; writing—review and editing, T.C., N.Y., X.Z., X.Y. and S.W.; visualization, T.C., N.Y. and S.W.; supervision, N.Y.; project administration, N.Y. and D.W.; funding acquisition, N.Y.; All authors have read and agreed to the published version of the manuscript.

**Funding:** This work was supported by the National Key Research and Development Program of China (2019YFC1904304), the University-Industry Collaborative Education Program of the Ministry of Education of China (202101255047), and the Fundamental Research Funds for the Central Universities (2022YQHH09).

**Institutional Review Board Statement:** Not applicable.

**Informed Consent Statement:** Not applicable.

**Data Availability Statement:** The data presented in this study are available on request from the corresponding author.

**Acknowledgments:** The authors are grateful to the School of Chemical and Environmental Engineering, China University of Mining and Technology (Beijing) for the experimental equipment and technical support.

**Conflicts of Interest:** The authors declare no conflict of interest.

## References

1. ACI 229R-13; Report on Controlled Low-Strength Materials. American Concrete Institute: Farmington Hills, MI, USA, 2013.
2. Somboonyanon, P.; Halmen, C. Seismic Behavior of Steel Pipeline Embedded in Controlled Low-Strength Material Subject to Reverse Slip Fault. *J. Pipeline Syst. Eng.* **2021**, *12*, 04021025. [[CrossRef](#)]
3. Alizadeh, V. Analytical study for allowable bearing pressures of CLSM bridge abutments. *Transp. Geotech.* **2019**, *21*, 100271. [[CrossRef](#)]
4. Do, T.M.; Kim, H.; Kim, M.; Kim, Y. Utilization of controlled low strength material (CLSM) as a novel grout for geothermal systems: Laboratory and field experiments. *J. Build. Eng.* **2020**, *29*, 101110. [[CrossRef](#)]
5. Bassani, M.; Bertola, F.; Bianchi, M.; Canonico, F.; Marian, M. Environmental assessment and geomechanical properties of controlled low-strength materials with recycled and alternative components for cements and aggregates. *Cem. Concr. Compos.* **2017**, *80*, 143–156. [[CrossRef](#)]
6. Mneina, A.; Soliman, A.M.; Ahmed, A.; El Naggar, M.H. Engineering properties of Controlled Low-Strength Materials containing Treated Oil Sand Waste. *Constr. Build. Mater.* **2018**, *159*, 277–285. [[CrossRef](#)]
7. Lee, N.K.; Kim, H.K.; Park, I.S.; Lee, H.K. Alkali-activated, cementless, controlled low-strength materials (CLSM) utilizing industrial by-products. *Constr. Build. Mater.* **2013**, *49*, 738–746. [[CrossRef](#)]
8. Hung, C.C.; Wang, C.C.; Wang, H.Y. Establishment of the Controlled Low-Strength Desulfurization Slag Prediction Model for Compressive Strength and Surface Resistivity. *Appl. Sci.* **2020**, *10*, 5674. [[CrossRef](#)]
9. Do, T.M.; Kang, G.O.; GO, G.H.; Kim, Y.S. Evaluation of Coal Ash-Based CLSM Made with Cementless Binder as a Thermal Grout for Borehole Heat Exchangers. *J. Mater. Civ. Eng.* **2019**, *31*, 04019072. [[CrossRef](#)]
10. Katz, A.; Kovler, K. Utilization of industrial by-products for the production of controlled low strength materials (CLSM). *Waste Manag.* **2004**, *24*, 501–512. [[CrossRef](#)]
11. Xiao, R.; Polaczyk, P.; Jiang, X.; Zhang, M.M.; Wang, Y.H.; Huang, B.S. Cementless controlled low-strength material (CLSM) based on waste glass powder and hydrated lime: Synthesis, characterization and thermodynamic simulation. *Constr. Build. Mater.* **2021**, *275*, 122157. [[CrossRef](#)]
12. Dueramae, S.; Sanboonsiri, S.; Suntadyon, T.; Aoudta, B.; Tangchirapat, W.; Jongpradist, P.; Pulngern, T.; Jitsangiam, P.; Jaturapitakkul, C. Properties of lightweight alkali activated controlled Low-Strength material using calcium carbide residue–Fly ash mixture and containing EPS beads. *Constr. Build. Mater.* **2021**, *297*, 123769. [[CrossRef](#)]
13. Zhen, G.Y.; Lu, X.Y.; Zhao, Y.C.; Niu, J.; Chai, X.L.; Su, L.H.; Li, Y.Y.; Liu, Y.; Du, J.R.; Hojo, T.; et al. Characterization of controlled low-strength material obtained from dewatered sludge and refuse incineration bottom ash: Mechanical and microstructural perspectives. *J. Environ. Manag.* **2013**, *129*, 183–189. [[CrossRef](#)]
14. Cheng, L.C.; Qin, Y.L.; Li, X.W.; Zhao, X.Y. A Laboratory and Numerical Simulation Study on Compression Characteristics of Coal Gangue Particles with Optimal Size Distribution Based on Shape Statistics. *Math. Probl. Eng.* **2020**, *2020*, 8046156. [[CrossRef](#)]
15. Jala, S.; Goyal, D. Fly ash as a soil ameliorant for improving crop production—A review. *Bioresour. Technol.* **2006**, *97*, 1136–1147. [[CrossRef](#)]
16. Dmitrienko, M.A.; Strizhak, P.A. Environmentally and economically efficient utilization of coal processing waste. *Sci. Total Environ.* **2017**, *598*, 21–27. [[CrossRef](#)]
17. Siddique, R. Utilization of coal combustion by-products in sustainable construction materials. *Resour. Conserv. Recycl.* **2010**, *54*, 1060–1066. [[CrossRef](#)]
18. Li, J.Y.; Wang, J.M. Comprehensive utilization and environmental risks of coal gangue: A review. *J. Clean. Prod.* **2019**, *239*, 117946. [[CrossRef](#)]
19. Miao, C.; Liang, L.X.; Zhang, F.; Chen, S.M.; Shang, K.X.; Jiang, J.L.; Zhang, Y.; Ouyang, J. Review of the fabrication and application of porous materials from silicon-rich industrial solid waste. *Int. J. Miner. Metall. Mater.* **2022**, *29*, 424–438. [[CrossRef](#)]
20. Gong, Y.B.; Sun, J.M.; Zhang, Y.M.; Zhang, Y.F.; Zhang, T.A. Dependence on the distribution of valuable elements and chemical characterizations based on different particle sizes of high alumina fly ash. *Fuel* **2021**, *291*, 120225. [[CrossRef](#)]
21. Zhang, Y.X.; Zheng, X.Z.; Cai, W.J.; Liu, Y.; Luo, H.L.; Guo, K.D.; Bu, C.J.; Li, J.; Wang, C. Key drivers of the rebound trend of China's CO<sub>2</sub> emissions. *Environ. Res. Lett.* **2020**, *15*, 104049. [[CrossRef](#)]
22. Volokitin, G.G.; Skripnikova, N.K.; Volokitin, O.G.; Lutsenko, A.V.; Shekhovtsov, V.V.; Litvinova, V.A.; Semenovykh, M.A. Bottom Ash Waste Used in Different Construction Materials. *IOP Conf. Ser. Mater. Sci. Eng.* **2017**, *189*, 012013. [[CrossRef](#)]
23. Wang, Y.L.; Zhao, Y.Q.; Han, Y.S.; Zhou, M. The Effect of Circulating Fluidised Bed Bottom Ash Content on the Mechanical Properties and Drying Shrinkage of Cement-Stabilised Soil. *Materials* **2022**, *15*, 14. [[CrossRef](#)]
24. Liu, R.; Vail, M.; Koohbor, B.; Zhu, C.; Tang, C.S.; Xu, H.; Shi, X.C. Desiccation cracking in clay-bottom ash mixtures: Insights from crack image analysis and digital image correlation. *Bull. Eng. Geol. Environ.* **2022**, *81*, 139. [[CrossRef](#)]
25. Pormmoon, P.; Abdulmatin, A.; Charoenwaiyachet, C.; Tangchirapat, W.; Jaturapitakkul, C. Effect of cut-size particles on the pozzolanic property of bottom ash. *J. Mater. Res. Technol.* **2021**, *10*, 240–249. [[CrossRef](#)]
26. González-Fontboa, B.; Carro-López, D.; Brito, J.D.; Martínez-Abella, F.; Seara-Paz, S.; Gutiérrez-Mainar, S. Comparison of ground bottom ash and limestone as additions in blended cements. *Mater. Struct.* **2017**, *50*, 84. [[CrossRef](#)]
27. Mazurkiewicz, M.; Tkaczewska, E.; Pomykala, R.; Uliasz-Bochenczyk, A. Preliminary determination of the suitability of slags resulting from coal gasification as a pozzolanic raw material. *Gospod. Surowcami Min.* **2012**, *28*, 5–14. [[CrossRef](#)]

28. Kaliyavaradhan, S.K.; Ling, T.C.; Guo, M.Z. Upcycling of wastes for sustainable controlled low-strength material: A review on strength and excavatability. *Environ. Sci. Pollut. Res.* **2022**, *29*, 16799–16816. [[CrossRef](#)]
29. Ling, T.C.; Kaliyavaradhan, S.K.; Poon, C.S. Global perspective on application of controlled low-strength material (CLSM) for trench backfilling—An overview. *Constr. Build. Mater.* **2018**, *158*, 535–548. [[CrossRef](#)]
30. Zhang, Q.L.; Wu, X.M. Performance of cemented coal gangue backfill. *J. Cent. South Univ.* **2007**, *14*, 216–219. [[CrossRef](#)]
31. Yang, X.B.; Yan, Z.P.; Yin, S.H.; Gao, Q.; Li, W.G. The Ratio Optimization and Strength Mechanism of Composite Cementitious Material with Low-Quality Fly Ash. *Gels* **2022**, *8*, 151. [[CrossRef](#)]
32. ASTM D6103-17; Standard Test Method for Flow Consistency of Controlled Low Strength Material (CLSM). ASTM International: West Conshohocken, PA, USA, 2017. Available online: [https://www.astm.org/d6103\\_d6103m-17.html](https://www.astm.org/d6103_d6103m-17.html) (accessed on 18 June 2022).
33. GB/T 50080-2016; Standard for Test Method of Performance on Ordinary Fresh Concrete. China National Standard, Ministry of Construction: Beijing, China, 2016.
34. GB/T 50081-2019; Standard for Test Method of Concrete Physical and Mechanical Properties. China National Standard, Ministry of Construction: Beijing, China, 2019.
35. GB/T 1346-2011; Test Methods for Water Requirement of Normal Consistency, Setting Time and Soundness of the Portland Cement. China National Standard, General Administration of Quality Supervision, Inspection and Quarantine: Beijing, China, 2011.
36. ASTM D6023-16; Standard Test Method for Density (Unit Weight), Yield, Cement Content, and Air Content (Gravimetric) of Controlled Low-Strength Material (CLSM). ASTM International: West Conshohocken, PA, USA, 2016. Available online: <https://www.astm.org/d6023-16.html> (accessed on 18 June 2022).
37. Yang, T.; Zhu, H.J.; Zhang, Z.H.; Gao, X.; Zhang, C.S.; Wu, Q.S. Effect of fly ash microsphere on the rheology and microstructure of alkali-activated fly ash/slag pastes. *Cem. Concr. Res.* **2018**, *109*, 198–207. [[CrossRef](#)]
38. Hwang, C.L.; Chiang, C.H.; Huynh, T.P.; Vo, D.H.; Jhang, B.J.; Ngo, S.H. Properties of alkali-activated controlled low-strength material produced with waste water treatment sludge, fly ash, and slag. *Constr. Build. Mater.* **2017**, *135*, 459–471. [[CrossRef](#)]
39. Chen, C.G.; Sun, C.J.; Gau, S.H.; Wu, C.W.; Chen, Y.L. The effects of the mechanical–chemical stabilization process for municipal solid waste incinerator fly ash on the chemical reactions in cement paste. *Waste Manag.* **2013**, *33*, 858–865. [[CrossRef](#)] [[PubMed](#)]
40. Li, H.; Chen, Y.; Cao, Y.; Liu, G.J.; Li, B.Q. Comparative study on the characteristics of ball-milled coal fly ash. *J. Therm. Anal. Calorim.* **2016**, *124*, 839–846. [[CrossRef](#)]
41. Rani, R.; Jain, M.K. Effect of bottom ash at different ratios on hydraulic transportation of fly ash during mine fill. *Powder Technol.* **2017**, *315*, 309–317. [[CrossRef](#)]
42. Yu, J.; Li, G.Y.; Leung, C.K.Y. Hydration and physical characteristics of ultrahigh-volume fly ash-cement systems with low water/binder ratio. *Constr. Build. Mater.* **2018**, *161*, 509–518. [[CrossRef](#)]
43. Andrade, L.B.; Rocha, J.C.; Cheriaf, M. Influence of coal bottom ash as fine aggregate on fresh properties of concrete. *Constr. Build. Mater.* **2009**, *23*, 609–614. [[CrossRef](#)]
44. Kim, M.H.; Choi, S.J. An Experimental Study on the Properties of Concrete using High Volume of Coal Ash. *Archit. Res.* **2002**, *4*, 39–44.
45. Singh, M.; Siddique, R. Strength properties and micro-structural properties of concrete containing coal bottom ash as partial replacement of fine aggregate. *Constr. Build. Mater.* **2014**, *50*, 246–256. [[CrossRef](#)]
46. Ghanad, D.A.; Soliman, A.; Godbout, S.; Palacios, J. Properties of bio-based controlled low strength materials. *Constr. Build. Mater.* **2020**, *262*, 120742. [[CrossRef](#)]
47. Singh, M.; Siddique, R. Properties of concrete containing high volumes of coal bottom ash as fine aggregate. *J. Clean. Prod.* **2015**, *91*, 269–278. [[CrossRef](#)]
48. Le, N.H.; Razakamanantsoa, A.; Nguyen, M.; Phan, V.T.; Dao, P.; Nguyen, D.H. Evaluation of physicochemical and hydromechanical properties of MSWI bottom ash for road construction. *Waste Manag.* **2018**, *80*, 168–174. [[CrossRef](#)]
49. Li, E.P.; Chen, H.Y.; Huang, F.L.; Tian, S.Q.; Yu, Z.Y. The bottom ash from municipal solid waste and sewage sludge co-pyrolysis technology: Characteristics and performance in the cement mortar and concrete. *IOP Conf. Ser. Earth Environ. Sci.* **2020**, *585*, 012091. [[CrossRef](#)]
50. Kwon, W.T.; Kim, B.I.; Kim, Y.; Kim, S.R.; Ha, S.W. Characterization of Power Plant Bottom Ash and its Application to Cement Mortar. *Mater. Sci. Forum* **2009**, *620–622*, 221–224. [[CrossRef](#)]
51. Ghanad, D.A.; Soliman, A.M. Bio-based alkali-activated controlled low strength material: Engineering properties. *Constr. Build. Mater.* **2021**, *279*, 122445. [[CrossRef](#)]
52. Kim, Y.S.; Do, T.M.; Kim, H.K.; Kang, G. Utilization of excavated soil in coal ash-based controlled low strength material (CLSM). *Constr. Build. Mater.* **2016**, *124*, 598–605. [[CrossRef](#)]
53. Jang, J.G.; Lee, N.K.; Lee, H.K. Fresh and hardened properties of alkali-activated fly ash/slag pastes with superplasticizers. *Constr. Build. Mater.* **2014**, *50*, 169–176. [[CrossRef](#)]
54. Lee, N.K.; Lee, H.K. Setting and mechanical properties of alkali-activated fly ash/slag concrete manufactured at room temperature. *Constr. Build. Mater.* **2013**, *47*, 1201–1209. [[CrossRef](#)]
55. Park, S.M.; Lee, N.K.; Lee, H.K. Circulating fluidized bed combustion ash as controlled low-strength material (CLSM) by alkaline activation. *Constr. Build. Mater.* **2017**, *156*, 728–738. [[CrossRef](#)]